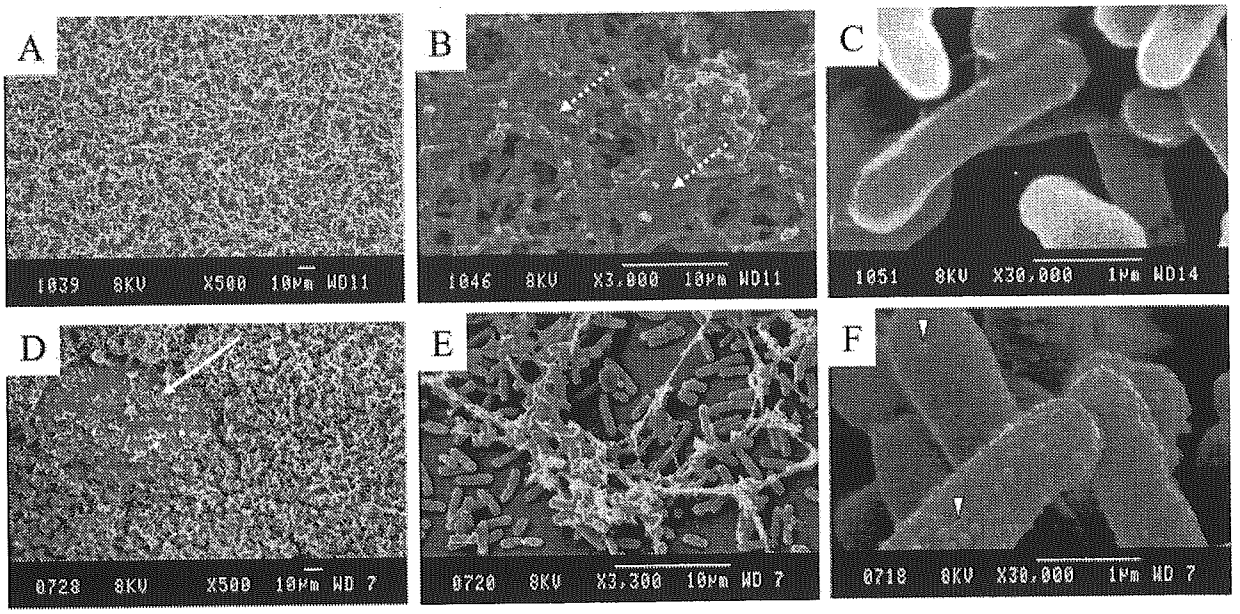

Figure 7. Scanning electron microscopy images of biofilm before (A, B, C) and after (D, E, F) exposure to 50 m*M* EGCg. The white arrow indicates the bare PU surface from which biofilm was detached. Dotted arrows indicate exopolysaccharides. White arrowheads indicate membrane vesicles.

shaped dark areas appeared here and there, indicating that biofilm was detached from the PU surface.

Scanning electron microscopy also revealed the morphological changes of biofilm formed on a glass slide. A biofilm which was harvested after 24-h incubation had a dense three-dimensional structure containing exopolysaccharides (EPS) produced as a matrix anchoring bacterial cells [Fig. 7(A,B)]. The higher magnification photo showed that the membrane surface of *E. coli* before EGCg exposure was smooth [Fig. 7(C)]. However, after EGCg (50 m*M*) was added to the medium, the dense structure of biofilm appeared to be degraded, and some parts of biofilm were detached from the surface and EPS completely disappeared [Fig. 7(D,E)]. The bacterial cell wall blebed off membrane vesicles [Fig. 7(F)].

Catechin-releasing bactericidal polymeric surfaces

EGCg-immobilized surfaces were prepared by photopolymerization of EGCg-mixed viscous liquid of photocurable biodegradable prepolymers, the chemical structures of which are shown in Figure 2. The time-dependent amounts of EGCg released from photocured biodegradable polymers coated onto the flat bottom of a glass bottle in PBS were determined using the Folin-Ciocalteu method. Figure 8(A) shows the time course of EGCg release from the photocured biodegradable polymers. The cumulative amount of released EGCg increased with time. The amount of released EGCg was largest for poly(TMC/LL/PEG1k), followed by poly(TMC/PEG200). It was the smallest for poly(TMC/TMP). This order is in good accordance with the order of hydrophilicity (wettabil-

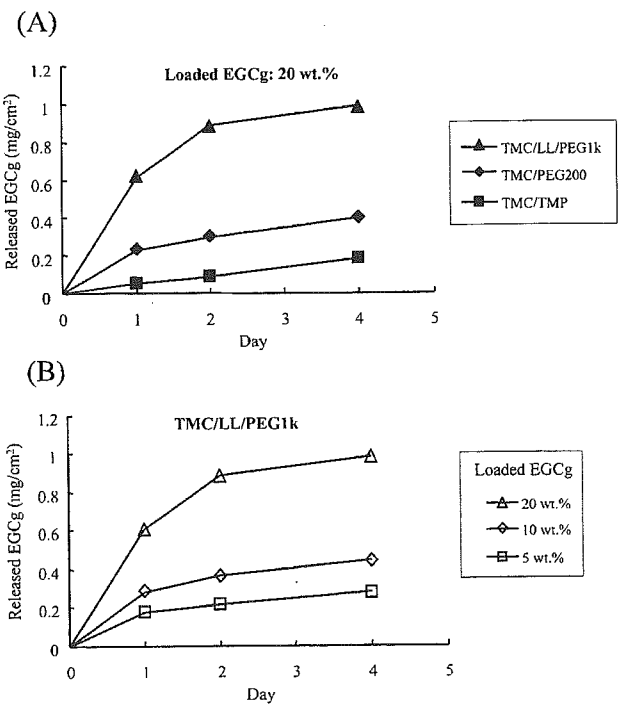

Figure 8. Time course of EGCg release from biodegradable polymers. (A) 20 wt % of EGCg is loaded in TMC/LL/PEG1k (▲), TMC/PEG200 (◆), and TMC/TMP(■). (B) 20 wt % (△), 10 wt % (◇), and 5 wt % (□) of EGCg is loaded in TMC/LL/PEG1k.

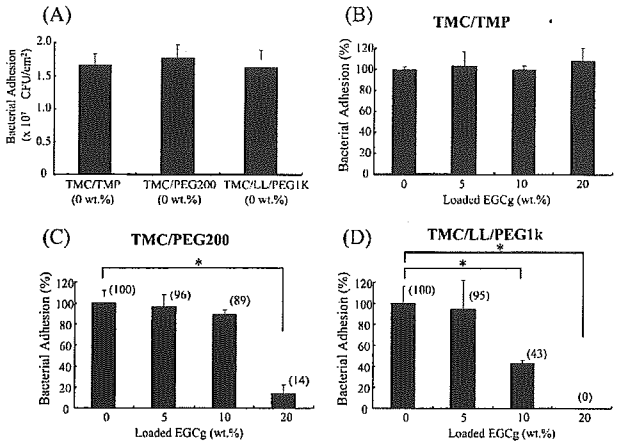

Figure 9. Bacterial adhesion of EGCg-loaded polymers under static conditions. (A) Non-EGCg-loaded polymers (TMC/TMP, TMC/PEG200, and TMC/LL/PEG1k). (B) TMC/TMP, (C) TMC/PEG200, and (D) TMC/LL/PEG1k loaded with 0, 5, 10, and 20 wt % of EGCg (n = 3). Data are presented as percentages relative to each respective non-EGCg-loaded polymer and shown as means ± SD.

ity toward water and swellability in water) (Table II). For EGCg-loaded poly(TMC/LL/PEG1k), enhanced releasing characteristics were observed with increasing loaded amount. Greater loading provides a higher release rate [Fig. 8(B)].

EGCg-loaded polymer discs coated on PU surfaces were incubated with *E. coli* (2×10^3 CFU/mL) for 24 h under static conditions, and, subsequently, adhered viable *E. coli* were counted by the plate count method. As shown in Figure 9, there is little difference in *E. coli* adhesion among the non-EGCg-loaded polymers listed above. For the least-swellable photocured polymer [poly(TMC/TMP)], irrespective of the amount of loading of EGCg, little difference in the number of adhered cells was observed. However, on the surfaces of 10- and 20-wt % EGCg-loaded poly(TMC/LL/PEG1k), and 20-wt % EGCg-loaded poly(TMC/PEG200), the adhesion was significantly inhibited compared with that on non-EGCg-loaded polymers. In particular, the 20-wt % EGCg-loaded poly(TMC/LL/PEG1k) surface completely inhibited the growth of *E. coli*. In confocal laser scanning microscopy, most of the surface areas of the nonloaded surface were green, which is derived from GFP-gene-encoded *E. coli* cells, whereas no *E. coli* cells were observed on the surface of the 20-wt % EGCg-loaded polymer surface (Fig. 10).

To study bacterial adhesion under flow conditions, the most swellable polymer [poly(TMC/LL/PEG1k)] with different degrees of EGCg loading (0–20 wt %) were coated on the sample ports of the flow-through device (MRD: Fig. 3). Then, medium containing *E. coli* (2×10^5 CFU/mL) was passed through the device for 1 h, followed by *E. coli*-free medium for 23 h. Then, the adhered *E. coli* cells were counted by the plate count method. Dose-dependent reduction of bacterial adhesion was noted similarly to that under static conditions [Fig. 9(D)]. The 20-wt % EGCg-loaded polymer completely prevented biofilm formation, similarly to that under static conditions. For 5-wt % EGCg-loaded polymer, a significant reduction of *E. coli* adhesion was observed (Fig. 11). The degree of adhesion of *E. coli* (19% to control) was much lower than that (95%) under nonflow (static) conditions [Fig. 9(D)].

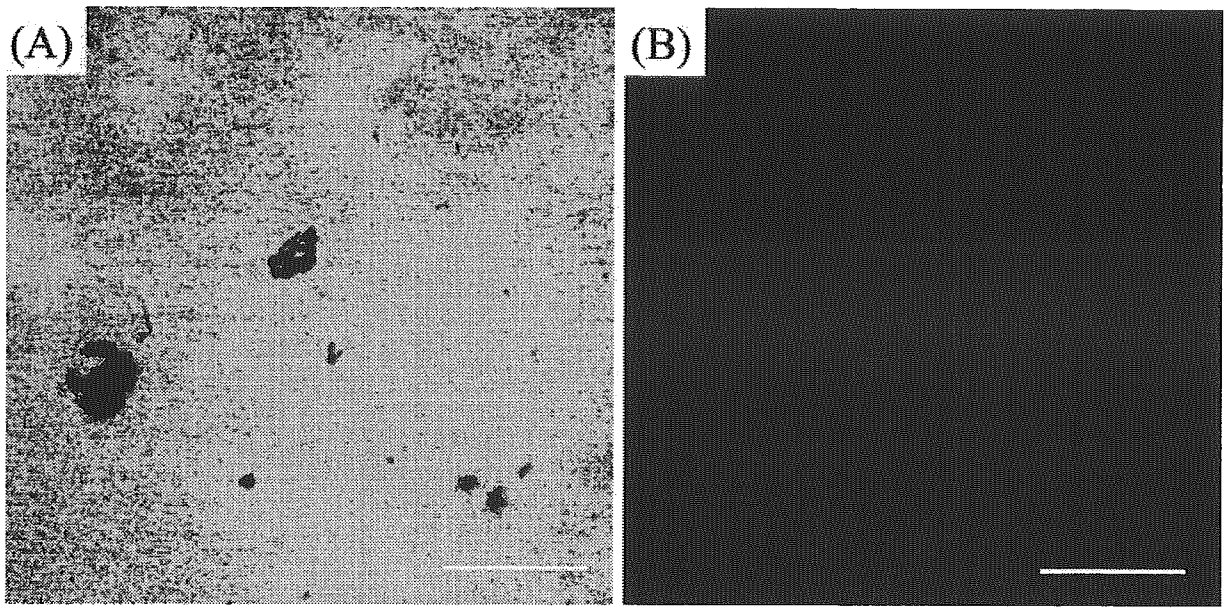

Figure 10. Confocal laser scanning microscopy of biofilm formed on the polymer surface. (A) TMC/LL/PEG1k without EGCg loading. (B) TMC/LL/PEG1k loaded with 20 wt % of EGCg. Bar: 500 μm.

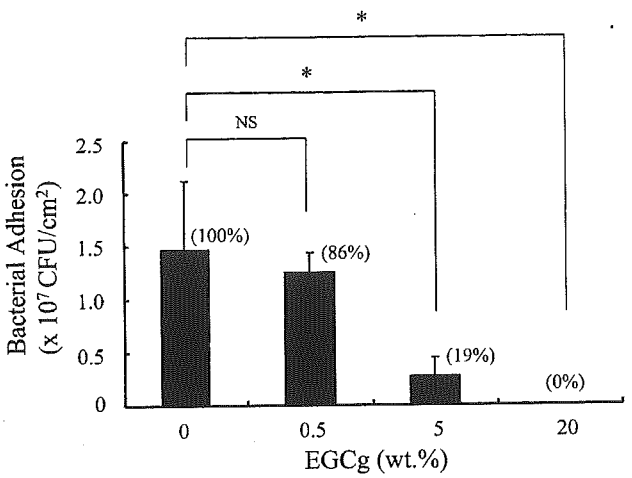

Figure 11. Bacterial adhesion on 0-, 0.5-, 5-, and 20-wt % EGCg-loaded polymers (TMC/LL/PEG1k) under flow conditions (n = 3). Data are shown as means ± SD.

DISCUSSION

Bacterial infection and colonization leading to biofilm formation remain major complications in implanted and percutaneous medical devices and is an important step in the pathogenesis of infection, which frequently causes septic complications. These devices include vascular catheters, prosthetic heart valves, peritoneal dialysis catheters, various types of stents (vascular, urinary, and biliary), and implanted orthopedic devices.[7,21] For example, infective endocarditis involving prosthetic heart valves is a potentially serious complication after heart-valve replacement surgery. High morbidity and mortality rates have been associated with biomaterial-centered infection despite aggressive antimicrobial therapy, thus leading to the need for surgical intervention in most cases. The mechanism of bacterial adhesion to implanted surfaces is a very complicated topic and remains unclear.[22] After adhering to the implanted surfaces, colonization and subsequent biofilm formation, accompanied with very rapid cell proliferation and secretion of slimy EPS, render the bacteria less accessible to the host defense systems and significantly decrease antibiotic susceptibility.[23]

Although antibacterial drug-loaded implants or catheters have been developed, the occurrence of drug-resistant bacteria or the unknown toxicity to the human body hampers the realization of "true" antibacterial surfaces.[10] In particular, increasing numbers of reports on various antibiotic-resistant bacteria indicate the worsening situation that we are facing in the battle against bacterial infections. The reason why we chose catechin, epigallocatechin gallate in particular, as a potential candidate for an bactericidal drug without substantial adverse effects is based on a recent report on the cytocidal activity of catechins toward Gram-negative and Gram-positive bacteria (Table I).

Catechins are polyphenol compounds extracted from tea, which is the most common drink served nearly every day to a vast majority of people in the world. EGCg, the main constituent of the tea catechins, interacts with and penetrates in the bacterial membrane or lipid bilayer, disrupting the barrier function, or binding to cell adhesive receptors as observed for cancer cells, both of which contribute to function as a potent bactericidal activity.[11,12] Interestingly, among the catechin family, the most phenol group-populated substance, EGCg exhibits outstandingly high bactericidal, anticancer, and antioxidative efficacy in contrast with the fact that (−)-epicatechin and (−)-epigallocatechin (both structures are shown in Fig. 1) have neither bactericidal nor anticancer effect.[12,24] EGCg is the only gallate (gallic acid ester), suggesting that the gallate moiety may be critical for bactericidal effect. As shown in Figure 3, the adhesion of *E. coli* to a PU surface was completely inhibited at EGCg concentrations >0.15 m*M*. However, to kill all *E. coli* in an established biofilm, which was harvested in EGCg-free medium for 24 h, nearly 50 m*M* of EGCg was necessary (Fig. 5). Bacteria present within an established biofilm has been reported to be more resistant to antibiotic therapy, and 100–1000 times the MIC level of an antibiotic is required to kill biofilm bacteria compared with the planktonic or free-floating bacterial form.[7,25] Our result coincides with this finding, and, therefore, exposure to catechin before bacterial adhesion and colonization seems to be much more effective for maintaining a biofilm-free surface.

Confocal laser scanning microscopic observation using fluoroprobed *E. coli* and fluorostaining of dead *E. coli* revealed the morphological change of biofilm with changing concentration of EGCg. The red regions, which were constructed of dead *E. coli* cells, and the yellowish regions, in which live and dead cells coexisted, increased with an increase in the concentration of EGCg (Fig. 6). At a high dose (20–50 m*M*) of EGCg, black regions which are identified as biofilm-detached spots, were observed by using scanning electron microscopy (Fig. 7). In high-magnification scanning electron microscopy images of samples subjected to EGCg exposure, EPS disappeared and *E. coli* blebed off the membrane surface to create membrane vesicles. Membrane vesicles release various degradation enzymes such as protease, alkaline phosphatase, and phospholipase C.[26] EPS lyase is usually released from biofilm bacteria under starvation conditions, which degrades the EPS that serves as a nutrient source for bacteria and hence contribute to biofilm detachment from the substrate. This is a bacterial survival strategy that has been established through billions of years of adaptation in hostile environments.[27] Taken together with our experimental results, it is hypothesized that EGCg

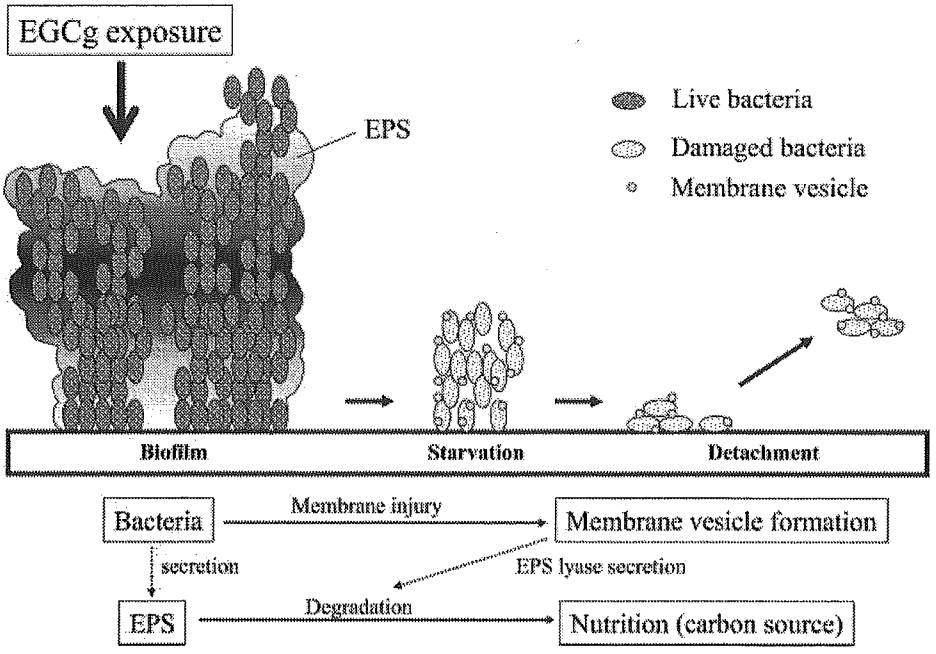

Figure 12. Schema of morphological change of biofilm exposed to EGCg. EPS, exopolysaccharide.

exposure induced the starvation of biofilm by damaging the bacterial membrane, as schematically shown in Figure 12.

The next step is to prevent biofilm formation on the foreign body surface of implanted devices. Our approach is to develop a local drug-releasing system aiming at combining the effects of the bactericidal activity of the naturally occurring nontoxic polyphenol, catechin, and wash-out of biofilm from the surface via surface erosion mechanism. Our previous study showed that the photocured polymers listed in Figure 2 are degraded via surface erosion, which were evidenced with various physicochemical analyses using confocal laser scanning microscopy and atomic force microscopy.[19] The amount of released EGCg depends on the polymer's surface characteristics; the higher the water wettability, water uptake or swellability and surface erosion rate is, the greater the amount of released EGCg [Fig. 8(A)]. In addition, the release rate of EGCg increased with the amount of loaded EGCg [Fig. 8(B)].

Many studies have revealed that a hydrophilic polymer surface significantly reduced the amount of adhered *E. coli*.[21] However, in this study, there was little significant effect on *E. coli* adhesion despite a diverse surface hydrophobicity/hydrophilicity balance in the absence of EGCg [Fig. 9(A)]. The bactericidal effect was enhanced with a more swellable, faster biodegradable polymer surface and with higher concentration of loaded EGCg. It is of interest to see that hydrodynamic shear stress reduced the amount of biofilm formation. For example, the amount of adhered bacteria on 5-wt %-loaded polymer was 95% under nonflow (static) conditions [Fig. 9(D)], and 19% under flow conditions (Fig. 11).

On the basis of these results, the following scenario of preventing biofilm formation and inducing biofilm degradation is presented using our proposed and prototype technology. The schema of such sustained releasing system via surface erosion mechanism is shown in Figure 13. Upon swelling at the surface region in a physiological fluid, some catechin is re-

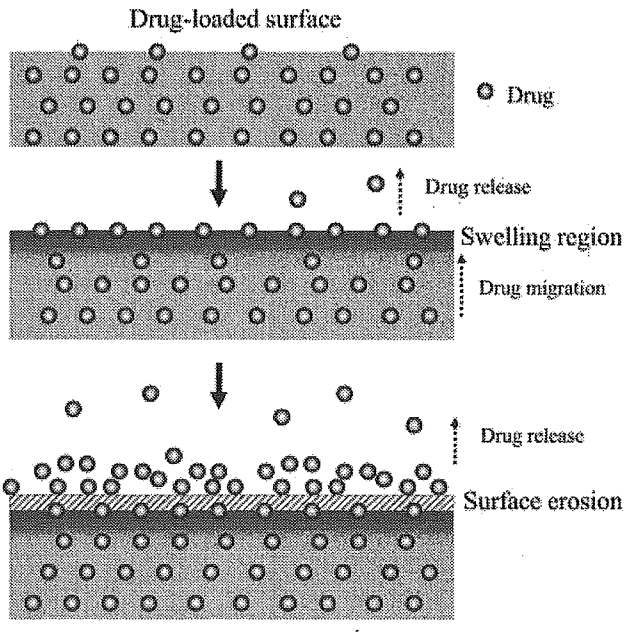

Figure 13. Schema of drug-releasing mechanism from hydrophilic biodegradable polymer.

leased from the swelling surface region, to which catechin had migrated from the bulk phase. As surface erosion proceeds with time, more catechin is released to the fluid, resulting in a very high local concentration of catechin in the interfacial region near the surface and catechin accumulation in the outermost surface region, both of which contribute to the destruction of the three-dimensional biofilm architecture as well as of the biofilm/substrate interface. In addition, the mechanically weakened interfacial region and whole body of biofilm cannot withstand the hydrodynamic shear stress of the physiological environment, resulting in detachment, removal, or washout of biofilm. All these phenomena contribute to biofilm destruction and removal. We are developing a long-life, sustainable biliary stent using this technique for patients with pancreatic cancer. The pharmacological effect of catechin and sustained release from surface-erodible polymer may contribute to the bactericidal effect of such coatings on the surface of a biliary stent, through which there is a continuous flow of bile (flow rate: approximately 0.4 mL/min).[28]

In conclusion, we developed a novel bactericidal surface from which EGCg is sustainably released upon surface erosion, resulting in the prevention of biofilm formation.

The authors thank T. Kanemaru for electron microscopic examination. This study was supported by a Grant-in-Aid for Scientific Research from the Ministry of Health, Labour and Welfare of Japan, the Ministry of Education, Culture, Sports, Science, and Technology of Japan (both for T. Matsuda), and NIH/NIBIB (for J. M. Anderson).

References

1. An YH, Friedman RJ. Concise review of mechanisms of bacterial adhesion to biomaterial surfaces. J Biomed Mater Res 1998;43:338–348.
2. Gristina AG. Biomaterial-centered infection: microbial adhesion versus tissue integration. Science 1987;237:1588–1595.
3. Davies D. Understanding biofilm resistance to antibacterial agents. Nat Rev Drug Discov 2003;2:114–122.
4. Tsang TK, Pollack J, Chodash HB. Inhibition of biliary endoprostheses occlusion by ampicillin-sulbactam in an *in vitro* model. J Lab Clin Med 1997;130:643–648.
5. Leung JW, Liu YL, Desta TD, Libby ED, Inciardi JF, Lam K. *In vitro* evaluation of antibiotic prophylaxis in the prevention of biliary stent blockage. Gastrointest Endosc 2000;51:296–303.
6. Klueh U, Wagner V, Kelly S, Johnson A, Bryers JD. Efficacy of silver-coated fabric to prevent bacterial colonization and subsequent device-based biofilm formation. J Biomed Mater Res 2000;53:621–631.
7. Leung JW, Liu Y, Cheung S, Chan RC, Inciardi JF, Cheng AF. Effect of antibiotic-loaded hydrophilic stent in the prevention of bacterial adherence: a study of the charge, discharge, and recharge concept using ciprofloxacin. Gastrointest Endosc 2001;53:431–437.
8. van de Belt H, Neut D, Schenk W, van Horn JR, van Der Mei HC, Busscher HJ. *Staphylococcus aureus* biofilm formation on different gentamicin-loaded polymethylmethacrylate bone cements. Biomaterials 2001;22:1607–1611.
9. Leung JW, Lau GT, Sung JJ, Costerton JW. Decreased bacterial adherence to silver-coated stent material: an *in vitro* study. Gastrointest Endosc 1992;38:338–340.
10. Yoda Y, Hu ZQ, Zhao WH, Shimamura T. Different susceptibilities of *Staphylococcus* and Gram-negative rods to epigallocatechin gallate. J Infect Chemother 2004;10:55–58.
11. Ikigai H, Nakae T, Hara Y, Shimamura T. Bactericidal catechins damage the lipid bilayer. Biochim Biophys Acta 1993;1147:132–136.
12. Tachibana H, Koga K, Fujimura Y, Yamada K. A receptor for green tea polyphenol EGCG. Nat Struct Mol Biol 2004;11:380–381.
13. Kondo K, Kurihara M, Miyata N, Suzuki T, Toyoda M. Mechanistic studies of catechins as antioxidants against radical oxidation. Arch Biochem Biophys 1999;362:79–86.
14. Zhao WH, Hu ZQ, Hara Y, Shimamura T. Inhibition by epigallocatechin gallate (EGCg) of conjugative R plasmid transfer in *Escherichia coli*. J Infect Chemother 2001;7:195–197.
15. Sung JY, Leung JW, Shaffer EA, Lam K, Costerton JW. Bacterial biofilm, brown pigment stone and blockage of biliary stents. J Gastroenterol Hepatol 1993;8:28–34.
16. Speer AG, Cotton PB, Rode J, Seddon AM, Neal CR, Holton J, Costerton JW. Biliary stent blockage with bacterial biofilm. A light and electron microscopy study. Ann Intern Med 1988;108:546–553.
17. Maeyama R, Mizunoe Y, Anderson JM, Tanaka M, Matsuda T. Confocal imaging of biofilm formation process using fluoroprobed *Escherichia coli* and fluoro-stained exopolysaccharide. J Biomed Mater Res 2004;70A:274–282.
18. Watanabe M, Inoue M, Mitsuhashi S. *In vitro* activity of amifloxacin against outer membrane mutants of the family *Enterobacteriaceae* and frequency of spontaneous resistance. Antimicrob Agents Chemother 1989;33:1837–1840.
19. Matsuda T, Kwon IK, Kidoaki S. Photocurable biodegradable liquid copolymers: synthesis of acrylate-end-capped trimethylene carbonate-based prepolymers, photocuring, and hydrolysis. Biomacromolecules 2004;5:295–305.
20. Pastrana Bonilla E, Akoh CC, Sellappan S, Krewer G. Phenolic content and antioxidant capacity of muscadine grapes. J Agric Food Chem 2003;51:5497–5503.
21. Jansen B, Goodman LP, Ruiten D. Bacterial adherence to hydrophilic polymer-coated polyurethane stents. Gastrointest Endosc 1993;39:670–673.
22. Merritt K, Gaind A, Anderson JM. Detection of bacterial adherence on biomedical polymers. J Biomed Mater Res 1998;39:415–422.
23. Higashi JM, Wang IW, Shlaes DM, Anderson JM, Marchant RE. Adhesion of *Staphylococcus epidermidis* and transposon mutant strains to hydrophobic polyethylene. J Biomed Mater Res 1998;39:341–350.
24. Amarowicz R, Pegg RB, Bautista DA. Antibacterial activity of green tea polyphenols against *Escherichia coli* K 12. Nahrung 2000;44:60–62.
25. Nickel JC, Wright JB, Ruseska I, Marrie TJ, Whitfield C, Costerton JW. Antibiotic resistance of *Pseudomonas aeruginosa* colonizing a urinary catheter *in vitro*. Eur J Clin Microbiol 1985;4:213–218.
26. Beveridge TJ, Makin SA, Kadurugamuwa JL, Li Z. Interactions between biofilms and the environment. FEMS Microbiol Rev 1997;20:291–303.
27. Allison DG, Ruiz B, SanJose C, Jaspe A, Gilbert P. Extracellular products as mediators of the formation and detachment of *Pseudomonas fluorescens* biofilms. FEMS Microbiol Lett 1998;167:179–184.
28. Hongo T, Hiroshige C. Hyoujunseirigaku (Text in Japanese) 1996;677–682.

Microbiol. Immunol., 49(9), 875–884, 2005

Editor-Communicated Paper

Curli Fibers Are Required for Development of Biofilm Architecture in *Escherichia coli* K-12 and Enhance Bacterial Adherence to Human Uroepithelial Cells

Tatsuya Kikuchi[1,2], Yoshimitsu Mizunoe*[,1], Akemi Takade[1], Seiji Naito[2], and Shin-ichi Yoshida[1]

[1]*Department of Bacteriology and* [2]*Department of Urology, Faculty of Medical Sciences, Kyushu University, Fukuoka, Fukuoka 812–8582, Japan*

Communicated by Dr. Motoyuki Sugai: Received June 14, 2005. Accepted June 28, 2005

Abstract: **Sessile bacteria show phenotypical, biochemical, and morphological differences from their planktonic counterparts. Curli, extracellular structures important for biofilm formation, are only produced at temperatures below 30 C in *Escherichia coli* K-12 strains. In this report, we show that *E. coli* K-12 can produce curli at 37 C when grown as a biofilm community. The curli-expressing strain formed more biofilms on polyurethane sheets than the curli-deficient strain under growth temperatures of both 25 C and 37 C. Curli are required for the formation of a three-dimensional mature biofilm, with characteristic water channels and pillars of bacteria. Observations by electron microscopy revealed the presence at the surfaces of the curli-deficient mutant in biofilm of flagella and type I pili. A wild-type curli-expressing *E. coli* strain significantly adhered to several lines of human uroepithelial cells, more so than an isogenic curli-deficient strain. The finding that curli are expressed at 37 C in biofilm and enhance bacterial adherence to mammalian host cells suggests an important role for curli in pathogenesis.**

Key words: ***Escherichia coli*, Biofilm, Curli, Adherence**

In natural settings, many bacteria are found as surface associated communities called biofilms (8, 12, 17). Bacteria growing as a biofilm develop significant phenotypical, biochemical, and morphological differences from their planktonic counterparts. This different biochemical and phenotypical behavior reflects different patterns of gene expression compared with planktonic cells (30, 32). Biofilms generate major health problems. Bacterial ability to colonize indwelling medical devices and low biofilm sensitivity to biocides and antibiotics lead to severe infections (7). The formation of mature biofilm architecture of several bacterial species has been described as a developmental differentiation process (25). The mature and differentiated three-dimensional structure of biofilms is characterized by mushroom or pillar shaped bacterial clusters surrounded by water channels allowing the influx of nutrients and the efflux of waste products (8, 9, 11, 19, 33, 40, 42). In contrast to the extensive characterization of biofilm structure, little is known about the molecular mechanisms underlying the maturation and differentiation of the biofilm. Several extracellular structures including lipopolysaccharide (41), flagella, pili (28) and other outer membrane adhesins (10, 28, 37, 40) are involved in the initial adhesion of bacterial cells to a solid surface. It has been reported that exopolysaccharide (EPS) synthesis is involved in the formation of three-dimensional biofilm architecture in several bacterial species; VPS exopolysaccharide in *V. cholerae* (23, 38, 40, 43), EPS colanic acid in *E. coli* (11) and EPS alginate in *Pseudomonas aeruginosa* (13, 18). Davies et al. (14) demonstrated that the cell-to-cell communica-

**Address correspondence to* Dr. Yoshimitsu Mizunoe, Department of Bacteriology, Faculty of Medical Sciences, Kyushu University, Fukuoka, Fukuoka 812–8582, Japan. Fax: +81–92–642–6133. E-mail: ymizunoe@bact.med.kyushu-u.ac.jp

Abbreviations: CFA, colonization factor antigen; CSLM, confocal scanning laser microscopy; CV, crystal violet; DAPI, 4′,6′-diamidino-2-phenylindole; EPS, exopolysaccharide.

tion mediated by an acylated homoserine lacton quorum-sensing signal molecule is required for *P. aeruginosa* to form mature biofilm. Acylhomoserine lactones were detected in biofilms formed on urethral catheters removed from patients (36) and on immersed stones from the San Marcos river in Texas (21). In contrast, cell-to-cell signaling mediated by autoinducer 2 (AI-2) is not required for *E. coli* biofilm development (33). Recently, other fiberous surface structures such as conjugative pili (15, 33) and curli (29, 37) have been shown to play an important role in biofilm formation of *E. coli* K-12 strains. Curli display direct interaction with the substratum and form interbacterial bundles, allowing a cohesive and stable association of cells in biofilm (31). The fertility pili, encoded by conjugative IncF plasmids are required for development and maturation of biofilm, whereas curli and other surface structures are all dispensable for biofilm maturation in chemostat cultures (33). Curli, known as thin aggregative fimbriae, are present in *E. coli* and *Salmonella* spp. (34, 35). Curli biogenesis is subject to tight and complex regulation; in *E. coli*, they are only produced at temperatures below 30 C, at low osmolarity, and in stationary phase (16, 20, 26). The biological function of curli remains to be solved. *In vitro* experiments suggest that curli are not expressed under conditions in mammalian hosts (37 C, high osmolarity). Therefore curli have not been considered to contribute to human infections, although curli have been implicated in binding to a variety of human host proteins including fibronectin, plasminogen and human contact phase proteins (4, 16, 27). It has been thought that curli may be involved in environmental survival, since conditions encountered outside the host enhance curli expression.

In this work, we investigated curli expression at various growth conditions and the role of curli in biofilm formation using *E. coli* K-12 YMel and its curli-deficient YMel-1 strains. This work shows that curli are expressed at 37 C when bacteria were grown in biofilm and are essential for biofilm maturation. We also show that curli enhance bacterial adherence to human uroepithelial cell lines, suggesting the contribution of curli to pathogenesis.

Materials and Methods

Bacterial strains, cell lines, and culture conditions. YMel, which is a curli-expressing wild-type *E. coli* K-12 strain (26), was used in this study. Generation of the curli-deficient mutant strain YMel-1 has been previously described (26). These strains were the generous gift of Dr. A. Arnqvist (Molecular Biology, Umea University, Sweden). Bacteria were grown on colonization factor antigen (CFA) agar plates (per liter, 10 g of Casamino Acids [Difco, Detroit, Mich., U.S.A.], 1.5 g of yeast extract [Difco], 50 mg of $MgSO_4$, 5 mg of $MnCl_2$, 2 g of Bacto agar [Difco] [pH 7.4]) (27) or in CFA liquid medium at 25 C or 37 C. T24 and KK47 cell lines, established from human transitional cell carcinomas of the urinary bladder, and SN12C, established from a human renal cell carcinoma, were maintained in minimal essential medium α medium (Gibco BRL, Grand Island, N.Y., U.S.A.) supplemented with 10% fetal bovine serum (FBS) (HyClone, Logan, Ut., U.S.A.) at 37 C in a 5% CO_2 atmosphere.

Growth of biofilms. For biofilm formation, bacteria were grown overnight in 5 ml of CFA medium at 37 C with shaking (150 rpm). 2.5 µl of the cultures was subcultured into 2.5 ml of CFA medium and incubated without shaking at 25 C and 37 C. When necessary, kanamycin was added at a concentration of 30 µg/ml.

Detection of curli expression. Expression of curli under various growth conditions was analyzed using an electron microscope. Electron microscopy was performed with a JEM 2000EX electron microscope (JEOL, Tokyo) with 100-mesh copper grids coated with thin films of 2% Formvar. Wild type *E. coli* K-12 YMel was grown on CFA plate or in CFA medium with shaking at both 25 C and 37 C. It was also grown in static CFA medium with polyethylene sheet to form biofilm. Samples grown on CFA plates were picked up and suspended with PBS and placed on the grid. Grids were washed twice with distilled water and negatively stained for 5 sec with 3.55% ammonium molybdate. Samples in CFA medium with shaking were directly picked up and placed on the grid. The samples grown in static CFA medium were rinsed three times with PBS and only adherent cells on the polyurethane sheets as biofilms were picked up and suspended in PBS and negatively stained.

Crystal violet (CV) analysis of bacterial cell attachment to polyurethane sheets. CV staining was performed as described previously (22) with a few modifications. Briefly, cultures of strains YMel and YMel-1 were grown in CFA medium in glass test tubes at 25 C or 37 C without shaking. Polyurethane sheets were put in each test tube. After 2, 4 and 7 days of growth, the polyurethane sheets were rinsed in distilled water, fixed with formalin for 5 min and then rinsed in distilled water. After the polyurethane sheets had been stained with 0.1% CV, rinsed and thoroughly dried, the CV was solubilized by the addition of 1 ml of 95% ethanol, and OD_{540} was determined using a SPECTRONIC GENESYS 5 (MILTON ROY, Ivyland, Penn., U.S.A.).

Scanning electron microscopy. Both YMel and YMel-1 strains were cultured in CFA medium at 25 C

and 37 C without shaking for 7 days. Polyurethane sheets were put into each glass test tube, as described in CV-analysis. After incubation, the biofilms growing on the sheets were sampled for scanning electron microscopy. The specimens were fixed with 2% glutaraldehyde in PBS for 1 hr, followed by 1% osmium tetroxide overnight at 4 C, dehydrated with a series of acetone concentrations ranging from 50% to 100%, dried by the critical point drying method, coated with gold-palladium for surface conductivity, and examined with a scanning image observing device (ASID) equipped with a JEM 2000EX electron microscope.

Transmission electron microscopy. The expression of the cell surface structures of YMel and YMel-1 strains in biofilm was examined by electron microscopy. *E. coli* strains were negatively stained and electron microscopy was performed as described above.

Confocal scanning laser microscopy (CSLM). Bacterial cell distribution in biofilm was determined after staining with 4',6'-diamidino-2-phenylindole (DAPI) (Sigma, St. Louis, Mo., U.S.A.). Both YMel and YMel-1 strains were cultured in CFA medium at 25 C without shaking for 7 days. Polyurethane sheets were put into each glass test tube as described above. After 7 days of growth, the polyurethane sheets were rinsed in distilled water and stained with 0.1 mg/ml of DAPI for 15 min. Confocal laser microscopy was conducted with a Radiance 2000 microscope (Bio-Rad, Hercules, Calif., U.S.A.) using a 488 nm excitation wavelength for visualization of the stained bacteria. Horizontal optical thin sections were collected and digitized by the LaserSharp 2000 software (Bio-Rad). These images were collected at 1.0-μm from the outer surface of the biofilm on the polyurethane sheet.

Adherence assay. Before the adherence assay, the tissue culture cells were incubated confluently in a 24-well plate. The number of confluent cells in an each well was 3.5×10^5 cells/well. A suspension of bacteria was added to the cells at the bacteria/cells ratio of 1,000/1, and the mixture was incubated for 3 hr at 37 C in 5% CO_2. After incubation, each well was rinsed three times in PBS, to remove the nonadherent bacteria. A solution of 0.5% deoxycol acid was then added to each well to release cells. Adherent bacteria were quantified by plating appropriate dilutions on Luria-Bertani (LB) agar plates (2).

Results

Expression of E. coli *Curli under Various Growth Conditions*

We investigated the expression of curli in *E. coli* K-12 YMel strain under various growth conditions. YMel cells were grown on CFA agar plates, in CFA medium with shaking, or in static CFA medium to form biofilms at 25 C and 37 C. Curli expression was analyzed by electron microscopy. Electron microscopic analysis revealed that all the samples of YMel cells grown at 25 C on CFA agar plates, in CFA medium with shaking or in static CFA medium, expressed curli (Table 1 and Fig. 1, a, c and e). On the other hand, when YMel was incubated at 37 C, bacteria from biofilm formed only after static growth expressed curli (Table 1 and Fig. 1f), but not on CFA agar plates nor in CFA medium with shaking (Table 1 and Fig. 1, b and d).

Biofilm Formation Assay

To evaluate the role of curli in *E. coli* K-12 biofilms, we compared the ability of a wild-type YMel strain and its isogenic *csgA* mutant YMel-1 strain for biofilm formation. YMel-1 is a *csgA::kan*^{R} chromosomal knockout mutant strain of *E. coli* YMel. The *csgA* gene encodes the curlin subunit. Test tubes containing 2.5 ml of CFA medium were inoculated either with YMel or with YMel-1 and a polyurethane sheet was put into each tube. Bacteria were grown at 25 C or 37 C. After 2, 4 and 7 days, each sheet was removed and stained with 0.1% crystal violet to quantify the biomass (see "Materials and Methods"). This assay revealed that the curli-expressing YMel strain formed more biofilms on polyurethane sheets than the curli-deficient YMel-1 strain under growth conditions at both 25 C or 37 C (Fig. 2).

Scanning Electron Microscopy

Scanning electron microscopy was used to visualize morphology of *E. coli* K-12 biofilms on polyurethane sheets. YMel or YMel-1 strain was incubated in static for 7 days at 25 C and 37 C. Under the condition grown at 25 C, YMel wild-type strain formed characteristic mushroom-like microcolonies (Fig. 3a), and produced an extracellular matrix possibly curli (Fig. 3c). In contrast, curli-deficient YMel-1 cells were not able to form complex three-dimensional structural biofilms and

Table 1. Expression of *E. coli* curli under various growth conditions

	Agar plate	Liquid medium	Biofilm
25 C	+	+	+
37 C	−	−	+

E. coli K-12 YMel cells were grown on CFA agar plates or in CFA medium with or without shaking at 25 C or 37 C. YMel cells were also grown in static with polyurethane sheets to form biofilm at 25 C or 37 C. +, curli expression positive; −, curli expression negative.

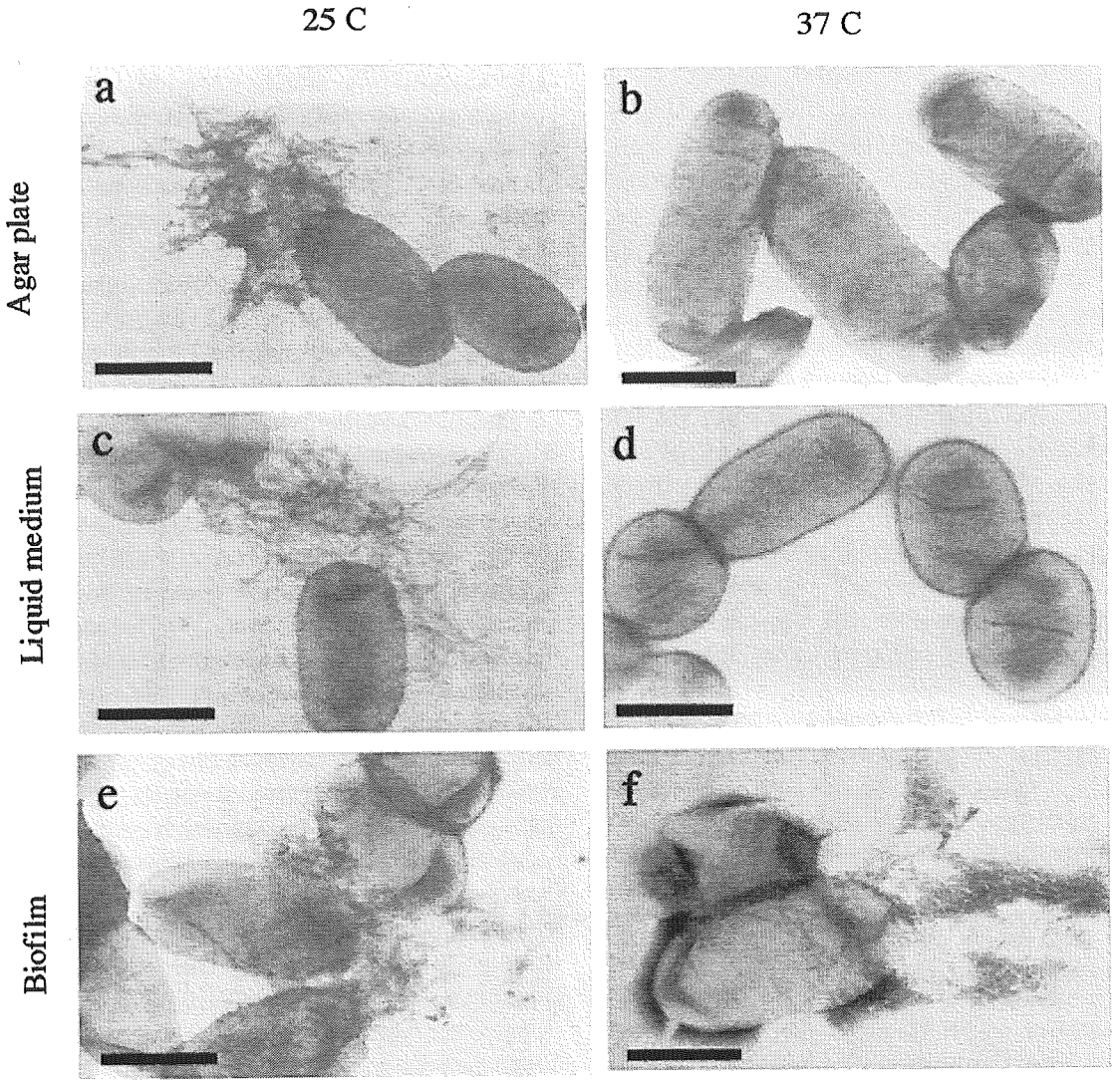

Fig. 1. Electron micrographs of negatively stained *E. coli* K-12 YMel. Bacteria were grown on CFA agar plates for 2 days (a and b), in CFA medium with shaking overnight (c and d), or in CFA medium under static condition for 4 days to form biofilm (e and f). The scale bars represent 500 nm.

an extracellular matrix was not observed (Fig. 3, b and d). Under the condition at 37 C, although YMel strain did not form mushroom-like, typical mature biofilms, it showed uneven structural biofilms (Fig. 3, e and g). In contrast, YMel-1 strain formed flat biofilms and produced little extracellular matrix (Fig. 3, f and h).

Confocal Scanning Laser Microscopy

CSLM analysis was performed to assess *E. coli* K-12 biofilm architecture developed on polyurethane sheets. YMel or YMel-1 strain was incubated in static at 25 C for 7 days and stained with DAPI. YMel wild-type strain formed many small microcolonies. The *z*-section image of wild-type strain showed an irregular three-dimensional structure separated by possible water channels (Fig. 4a). In contrast, YMel-1 strain did not form small microcolonies and formed flat biofilms. The *z*-section image of curli-deficient strain showed the tightly packed structure as continuous sheets (Fig. 4b).

The Expression of Cell Surface Structures

To study the differences of the expression of cell surface structures between a curli-expressing and a curli-deficient strain in biofilms, YMel and YMel-1 bacteria were observed by negatively stained electron microscopy. Wild-type YMel cells in biofilm expressed curli. Other cell surface structures were not observed in YMel strain (Fig. 5a). On the other hand, no curli were visualized, instead, flagella and pili were expressed in YMel-1 strain (Fig. 5b).

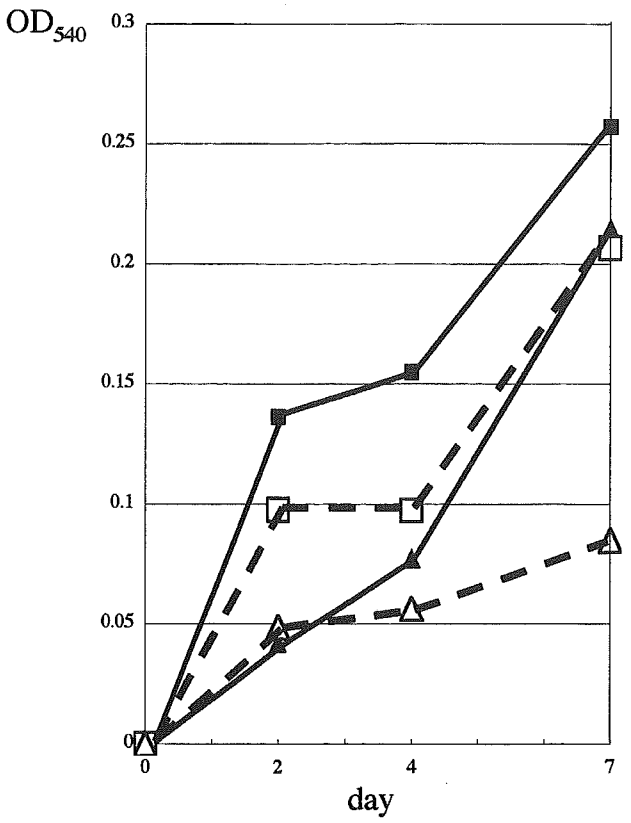

Fig. 2. Quantification of biofilm formation. YMel and YMel-1 bacteria were grown as described in "Materials and Methods." At each time point, polyurethane sheets were rinsed, stained with CV and the amount of CV staining was quantified to measure OD_{540}. Filled square, YMel grown at 25 C; open square, YMel grown at 37 C; filled triangle, YMel-1 grown at 25 C; open triangle, YMel-1 grown at 37 C. The experiments were repeated at least thrice; one representative experiment is shown.

Adherence Assay

The ability of strains YMel and YMel-1 to adhere to T24, KK47 and SN12C, three types of uroepithelial cells, was examined. The results are shown in Fig. 6. Wild-type YMel strain significantly adhered to all uroepithelial cells tested, more so than curli-deficient YMel-1 strain. These results suggested that curli enhanced bacterial adherence to mammalian host cells.

Discussion

Many microbes persist in attaching themselves to solid surfaces in communities generally referred to as biofilms. The term biofilm is used to describe matrix-enclosed microbial populations adherent to each other and to surfaces or interfaces (8). The mechanisms by which *E. coli* develop highly organized and mature biofilm structures are not well understood. Flagella, type I pili, and exopolysaccharide (EPS) have been implicated as important for biofilm formation in *E. coli* (11, 28, 37). Flagella are important for both initial interaction with the surface and for movement along the surface (28). Type I pili are required for initial surface attachment (28). EPS seems to be important for the formation of complex three-dimensional structure and persistence on biofilms (11). Recently, curli and conjugative pili have been shown to play important roles in *E. coli* biofilm formation (15, 29, 33, 37). The expression of gene coding for curli fibers is complex and involves several control elements, such as H-NS, RpoS, and OmpR (3). It has been reported that curli fibers are expressed after growth at 26 C but not at 37 C in *E. coli* (27). It has been thought that a low temperature-induced protein Crl regulates curli expression as a thermosensor (5). We investigated the expression of curli under various growth conditions. Curli were expressed under all growth conditions tested in this work, when bacteria were grown at 25 C. We found that bacteria expressed curli at 37 C when grown on solid surfaces to form biofilm, but not with shaking or on the agar plate. Biofilm-growing cells display different patterns of gene expression when compared with planktonic cells (32). The transcription of 38% of the *E. coli* genes was affected within biofilms. Different cell functions were more expressed in sessile bacteria: the OmpC porin, the high-affinity transport system of glycine betaine (encoded by proU operon), the colanic acid exopolysaccharide (*wca* locus, formerly called *cps*), tripeptidase T (*pepT*), and the nickel high-affinity transport system (*nikA*). On the other hand, the synthesis of flagellin (*fliC*) and a putative protein of 92 amino acids (f92) were both reduced in biofilms (32). The cell-to-cell signaling mechanisms and microenvironmental conditions of osmolarity and oxygen concentration can be correlated with this major change in gene expression (32). Our results may reflect that low oxygen concentration in biofilm conditions can be responsible for curli expression. In addition to the changes in multiple environmental physicochemical conditions, the adhesion event itself might have stimulated of the expression of curli at 37 C in biofilm.

We investigated the role of curli in *E. coli* K-12 biofilm formation using a wild-type YMel strain and its curli-deficient YMel-1 strain. YMel strain produced an extracellular matrix and formed mushroom-like or pillar-like, mature and differentiated biofilms. In contrast, YMel-1 strain produced little extracellular matrix and formed flat and tightly packed biofilm. Our data demonstrated that curli are required for the maturation of biofilm. Recently, several studies have shown that curli or other cell surface structures play an important role in biofilm formation and development in *E. coli* K-

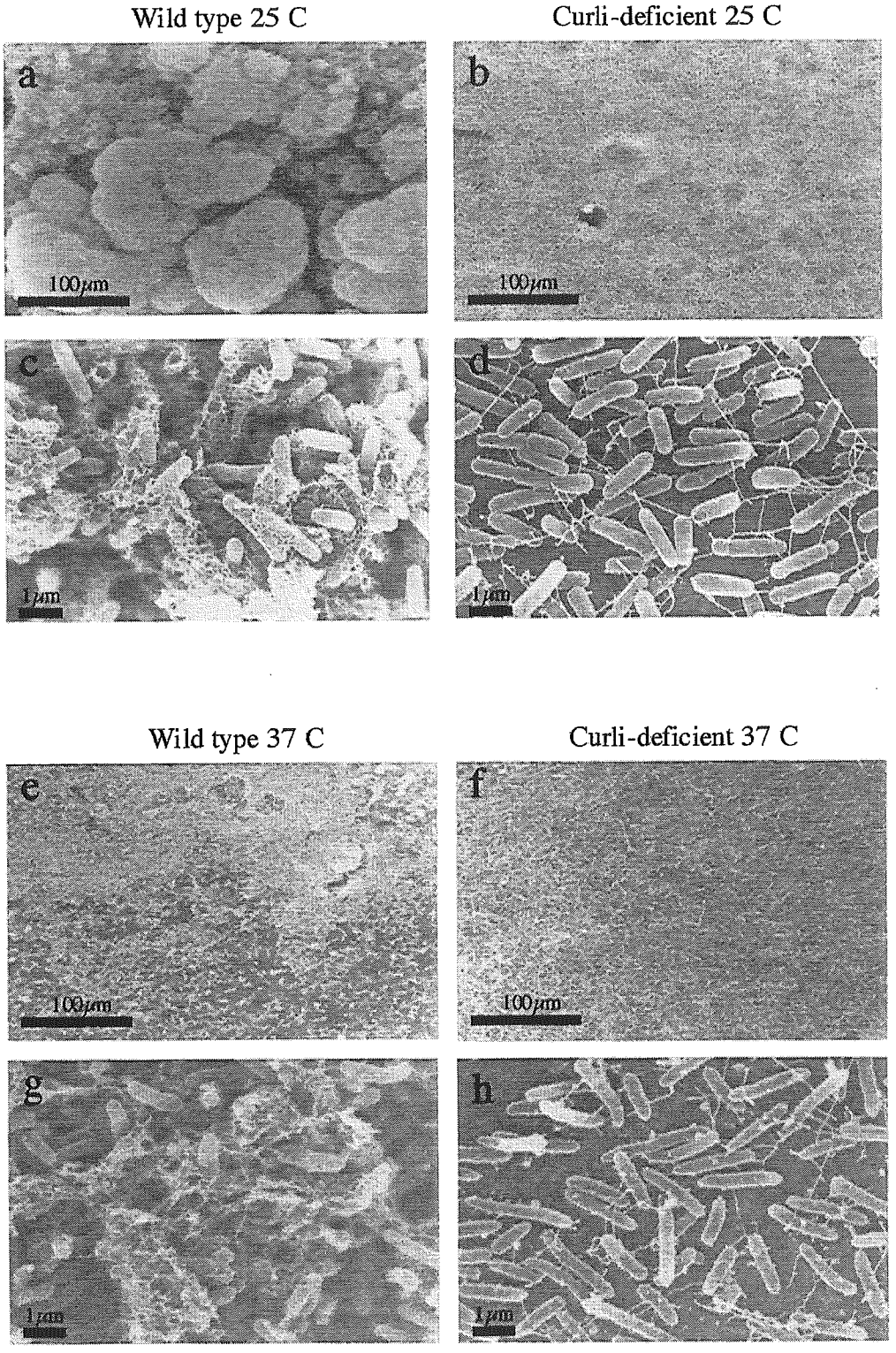

Fig. 3. Scanning electron micrographs of *E. coli* K-12 biofilm on polyurethane sheets. Bacteria were grown under static condition at 25 C and 37 C for 7 days. a to d, grown at 25 C; e to h, grown at 37 C. a, c, e and g, wild-type YMel strain; b, d, f and h, curli-deficient YMel-1 strain. a, b, e and f, the bar represents 100 μm; c, d, g and h, the bar represents 1 μm.

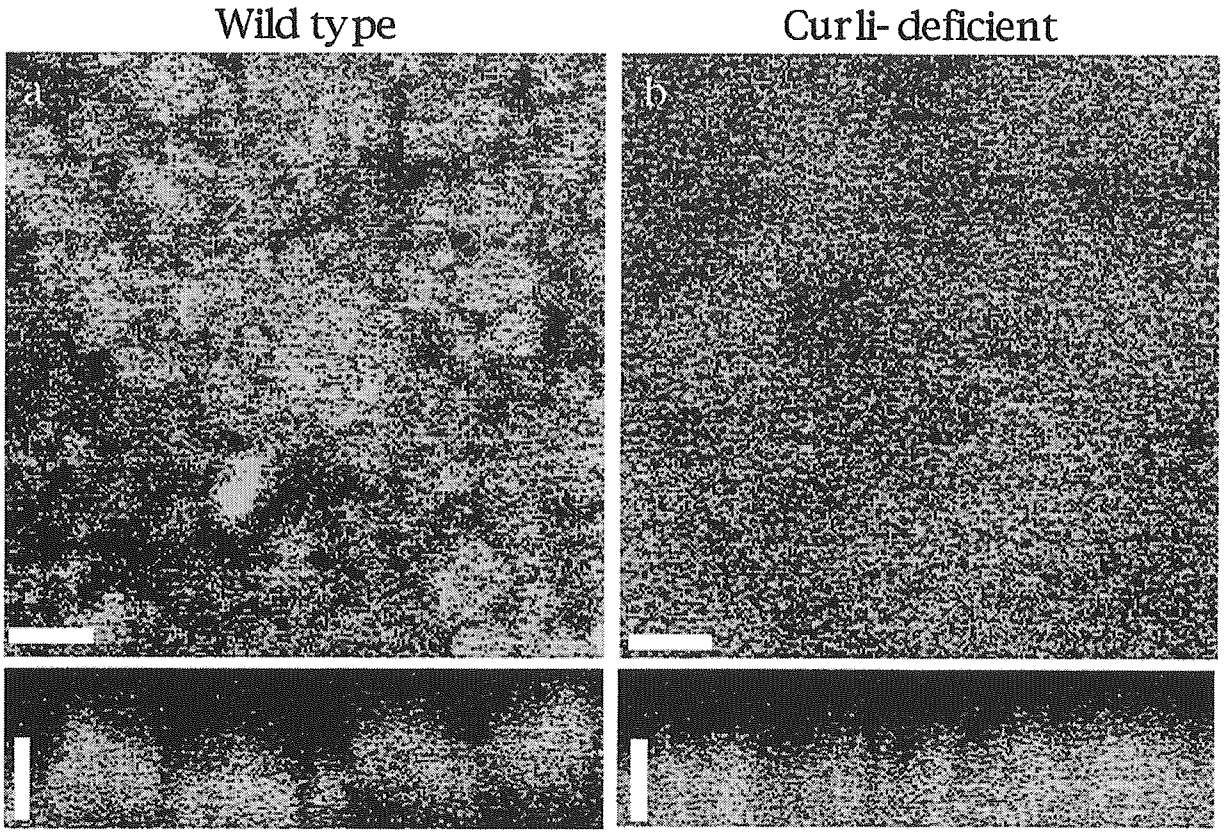

Fig. 4. Overhead and sagittal images of wild-type YMel (a) and curli-deficient YMel-1 (b) biofilms formed on polyurethane sheets. Bacteria were grown under static condition at 25 C for 7 days and stained with DAPI. Representative images of biofilms are shown. The scale bars represent 50 μm.

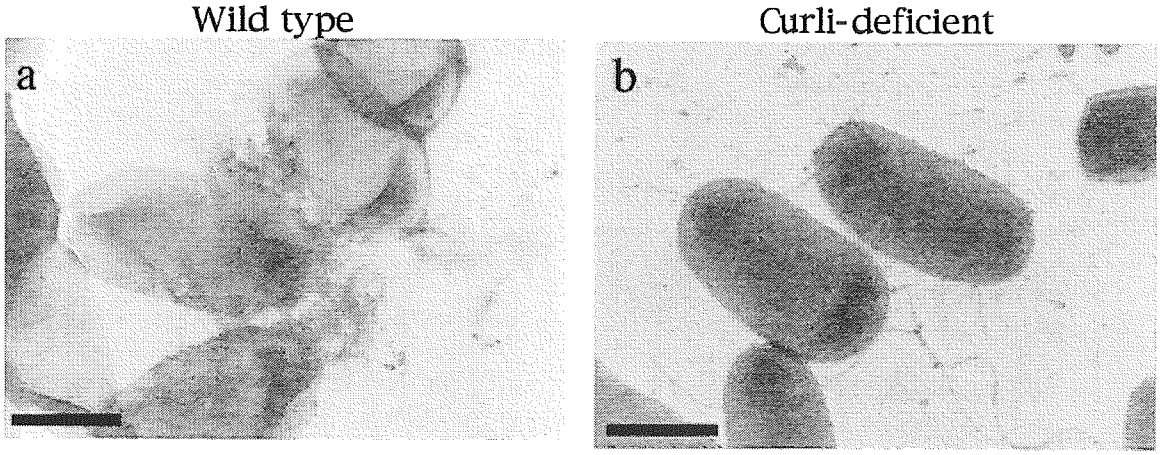

Fig. 5. Electron micrographs of negatively stained wild-type YMel (a) and curli-deficient YMel-1 (b) cells from biofilm formed on polyurethane sheets. Bacteria were grown under static condition at 25 C for 7 days. The scale bars represent 500 nm.

12 (11, 31, 33). Danese et al. (10) showed that colanic acid is critical for the formation of the complex three-dimensional structure and depth of *E. coli* biofilms. Reisner et al. (33) reported that presence of transfer constitutive IncF plasmids induced biofilm development forming mature structures resembling those reported for *Pseudomonas aeruginosa*, while flagella, type I fimbriae, curli and Ag43 are all dispensable for the *E. coli* biofilm maturation. These results may be influenced by differences in growth conditions such as static culture or flow cell culture. This suggests that biofilm maturation may require complex genetic control of the develop-

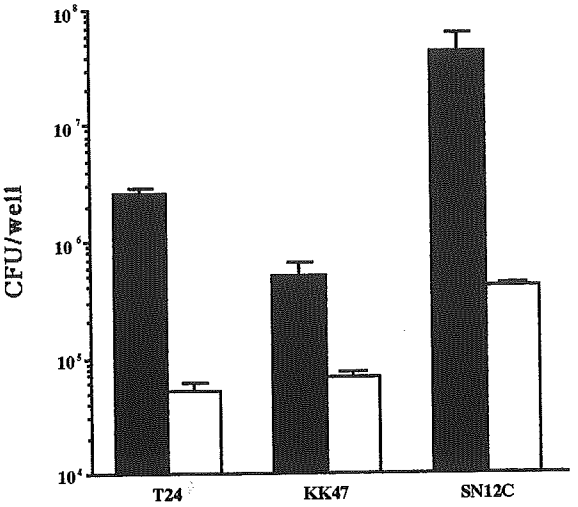

Fig. 6. Adhesion of *E. coli* to uroepithelial cells. The number of CFUs per well on each uroepithelial cell line is shown. Filled square represents adherence of YMel strain. Open square represents adherence of Ymel-1 strain. Bacteria and tissue culture cells were prepared as described in "Materials and Methods." The data are means±SD of three separate experiments.

mental process and multiple activities in bacterial cells.

It is supposed that the expression of *E. coli* genes, especially surface structure related genes, is changing step by step during the development, differentiation and maturation of biofilm. We performed electronmicroscopy to analyze the expression of cell surface structures of bacteria grown, in biofilm, using wild-type K-12 YMel and its isogenic curli-deficient YMel-1 strains. Electron microscopic examinations revealed that curli are expressed in YMel biofilm. However no type I pili or flagella could be detected in YMel sessile bacteria. We demonstrated that flagella and type I pili continued to be expressed even after 7 days incubation in a curli-deficient YMel-1 biofilm. We first show that flagella and type I pili are expressed to form biofilm when curli are not expressed.

We demonstrated that curli promote bacterial adherence to several lines of human uroepithelial cells. The structural gene encoding the curlin subunit is present in most wild-type isolates of *E. coli*, but the level of expression varies considerably between different isolates and clinical types (26). It has been reported that enterohemorrhagic, enterotoxigenic, and sepsis isolates express curli at 26 C and retain low expression of curli when grown at 37 C *in vitro*. Enteroinvasive and enteropathogenic isolates, on the other hand, express little or no curli at either temperature (4). Recently it has been realized that the majority of human bacterial infections are biofilm related (6, 24). Anderson et al. (1) reported that *E. coli* formed the intracellular biofilm-like pods in urinary tract infections of mice. Devices such as catheters and stents implanted into the urinary tract are particularly vulnerable to colonization by biofilms (39). Although not yet formally demonstrated, observations of this kind support the notion that curli could indeed be expressed by *E. coli* growing *in vivo*, especially in biofilm, where environmental conditions and selective pressures are considerably different from *in vitro* conditions. Thus, once expressed, curli will have the capacity to interact with human cells at physiological temperatures and contribute to the pathophysiology of bacterial infectious disease.

So far, most studies on biofilm formation and biofilm related gene expression in *E. coli* have been performed below 30 C. Further investigation of biofilm at physiological temperatures will hopefully provide a better understanding of the mechanisms on biofilm formation and of the contribution of biofilm to human bacterial infections.

We thank R. Maeyama, N. Hakoda and H. Kajiwara for technical assistance. We wish to thank L. Saza for manuscript preparation. This work was supported by Grants-in-Aid for Scientific Research (B) (2) 14370094, (B) (1) 12490009 and (C) (2) 15590391 from the Ministry of Education, Culture, Sports, Science and Technology, Japan.

References

1) Anderson, G.G., Palermo, J.J., Schilling, J.D., Roth, R., Heuser, J., and Hultgren, S.J. 2003. Intracellular bacterial biofilm-like pods in urinary tract infections. Science **301**: 105–107.
2) Archimbaud, C., Shankar, N., Forestier, C., Baghdayan, A., Gilmore, M.S., Charbonne, F., and Joly, B. 2002. *In vitro* adhesive properties and virulence factors of *Enterococcus faecalis* strains. Res. Microbiol. **153**: 75–80.
3) Arnqvist, A., Olsen, A., and Normark, S. 1994. Sigma S-dependent growth-phase induction of the *csgBA* promoter in *Escherichia coli* can be achieved *in vivo* by sigma 70 in the absence of the nucleoid-associated protein H-NS. Mol. Microbiol. **13**: 1021–1032.
4) Ben Nasr, A., Olsen, A., Sjobring, U., Muller-Esterl, W., and Bjorck, L. 1996. Assembly of human contact phase proteins and release of bradykinin at the surface of curli-expressing *Escherichia coli*. Mol. Microbiol. **20**: 927–935.
5) Bougdour, A., Lelong, C., and Geiselmann, J. 2004. Crl, a low temperature-induced protein in *Escherichia coli* that binds directly to the stationary phase sigma subunit of RNA polymerase. J. Biol. Chem. **279**: 19540–19550.
6) Costerton, J.W. 2001. Cystic fibrosis pathogenesis and the role of biofilms in persistent infection. Trends Microbiol. **9**: 50–52.
7) Costerton, J.W., Cheng, K.J., Geesey, G.G., Ladd, T.I., Nickel, J.C., Dasgupta, M., and Marrie, T.I. 1987. Bacterial biofilms in nature and disease. Annu. Rev. Microbiol. **41**: 435–464.

8) Costerton, J.W., Lewandowski, Z., Caldwell, D.E., Korber, D.R., and Lappin-Scott, H.M. 1995. Microbial biofilms. Annu. Rev. Microbiol. **49**: 711–745.
9) Costerton, J.W., Stewart, P.S., and Greenberg, E.P. 1999. Bacterial biofilms: a common cause of persistent infections. Science **284**: 1318–1322.
10) Danese, P.N., Pratt, L.A., Dove, S.L., and Kolter, R. 2000. The outer membrane protein, antigen 43, mediates cell-to-cell interactions within *Escherichia coli* biofilms. Mol. Microbiol. **37**: 424–432.
11) Danese, P.N., Pratt, L.A., and Kolter, R. 2000. Exopolysaccharide production is required for development of *Escherichia coli* K-12 biofilm architecture. J. Bacteriol. **182**: 3593–3596.
12) Davey, M.E., and O'Toole, G.A. 2000. Microbial biofilms: from ecology to molecular genetics. Microbiol. Mol. Biol. Rev. **64**: 847–867.
13) Davies, D.G., Chakrabarty, A.M., and Geesey, G.G. 1993. Exopolysaccharide production in biofilms: substratum activation of alginate gene expression by *Pseudomonas aeruginosa*. Appl. Environ. Microbiol. **59**: 1181–1186.
14) Davies, D.G., Parsek, M.R., Pearson, J.P., Iglewski, B.H., Costerton, J.W., and Greenberg, E.P. 1998. The involvement of cell-to-cell signals in the development of a bacterial biofilm. Science **280**: 295–298.
15) Ghigo, J.M. 2001. Natural conjugative plasmids induce bacterial biofilm development. Nature **412**: 442–445.
16) Hammar, M., Arnqvist, A., Bian, Z., Olsen, A., and Normark, S. 1995. Expression of two *csg* operons is required for production of fibronectin- and congo red-binding curli polymers in *Escherichia coli* K-12. Mol. Microbiol. **18**: 661–670.
17) Hinsa, S.M., Espinosa-Urgel, M., Ramos, J.L., and O'Toole, G.A. 2003. Transition from reversible to irreversible attachment during biofilm formation by *Pseudomonas fluorescens WCS365* requires an ABC transporter and a large secreted protein. Mol. Microbiol. **49**: 905–918.
18) Hoyle, B.D., Williams, L.J., and Costerton, J.W. 1993. Production of mucoid exopolysaccharide during development of *Pseudomonas aeruginosa* biofilms. Infect. Immun. **61**: 777–780.
19) Kierek, K., and Watnick, P.I. 2003. Environmental determinants of *Vibrio cholerae* biofilm development. Appl. Environ. Microbiol. **69**: 5079–5088.
20) Maurer, J.J., Brown, T.P., Steffens, W.L., and Thayer, S.G. 1998. The occurrence of ambient temperature-regulated adhesins, curli, and the temperature-sensitive hemagglutinin tsh among avian *Escherichia coli*. Avian Dis. **42**: 106–118.
21) McLean, R.J., Whiteley, M., Stickler, D.J., and Fuqua, W.C. 1997. Evidence of autoinducer activity in naturally occurring biofilms. FEMS Microbiol. Lett. **154**: 259–263.
22) Merritt, K., Gaind, A., and Anderson, J.M. 1998. Detection of bacterial adherence on biomedical polymers. J. Biomed. Mater. Res. **39**: 415–422.
23) Mizunoe, Y., Wai, S.N., Takade, A., and Yoshida, S.I. 1999. Isolation and characterization of rugose form of *Vibrio cholerae* O139 strain MO10. Infect. Immun. **67**: 958–963.
24) Morris, N.S., Stickler, D.J., and McLean, R.J. 1999. The development of bacterial biofilms on indwelling urethral catheters. World J. Urol. **17**: 345–350.
25) O'Toole, G., Kaplan, H.B., and Kolter, R. 2000. Biofilm formation as microbial development. Annu. Rev. Microbiol. **54**: 49–79.
26) Olsen, A., Arnqvist, A., Hammar, M., Sukupolvi, S., and Normark, S. 1993. The RpoS sigma factor relieves H-NS-mediated transcriptional repression of *csgA*, the subunit gene of fibronectin-binding curli in *Escherichia coli*. Mol. Microbiol. **7**: 523–536.
27) Olsen, A., Jonsson, A., and Normark, S. 1989. Fibronectin binding mediated by a novel class of surface organelles on *Escherichia coli*. Nature **338**: 652–655.
28) Pratt, L.A., and Kolter, R. 1998. Genetic analysis of *Escherichia coli* biofilm formation: roles of flagella, motility, chemotaxis and type I pili. Mol. Microbiol. **30**: 285–293.
29) Prigent-Combaret, C., Brombacher, E., Vidal, O., Ambert, A., Lejeune, P., Landini, P., and Dorel, C. 2001. Complex regulatory network controls initial adhesion and biofilm formation in *Escherichia coli* via regulation of the *csgD* gene. J. Bacteriol. **183**: 7213–7223.
30) Prigent-Combaret, C., and Lejeune, P. 1999. Monitoring gene expression in biofilms. Methods Enzymol. **310**: 56–79.
31) Prigent-Combaret, C., Prensier, G., Le Thi, T.T., Vidal, O., Lejeune, P., and Dorel, C. 2000. Developmental pathway for biofilm formation in curli-producing *Escherichia coli* strains: role of flagella, curli and colanic acid. Environ. Microbiol. **2**: 450–464.
32) Prigent-Combaret, C., Vidal, O., Dorel, C., and Lejeune, P. 1999. Abiotic surface sensing and biofilm-dependent regulation of gene expression in *Escherichia coli*. J. Bacteriol. **181**: 5993–6002.
33) Reisner, A., Haagensen, J.A., Schembri, M.A., Zechner, E.L., and Molin, S. 2003. Development and maturation of *Escherichia coli* K-12 biofilms. Mol. Microbiol. **48**: 933–946.
34) Romling, U., Bian, Z., Hammar, M., Sierralta, W.D., and Normark, S. 1998. Curli fibers are highly conserved between *Salmonella typhimurium* and *Escherichia coli* with respect to operon structure and regulation. J. Bacteriol. **180**: 722–731.
35) Romling, U., Sierralta, W.D., Eriksson, K., and Normark, S. 1998. Multicellular and aggregative behaviour of *Salmonella typhimurium* strains is controlled by mutations in the *agfD* promoter. Mol. Microbiol. **28**: 249–264.
36) Stickler, D.J., Morris, N.S., McLean, R.J., and Fuqua, C. 1998. Biofilms on indwelling urethral catheters produce quorum-sensing signal molecules *in situ* and *in vitro*. Appl. Environ. Microbiol. **64**: 3486–3490.
37) Vidal, O., Longin, R., Prigent-Combaret, C., Dorel, C., Hooreman, M., and Lejeune, P. 1998. Isolation of an *Escherichia coli* K-12 mutant strain able to form biofilms on inert surfaces: involvement of a new *ompR* allele that increases curli expression. J. Bacteriol. **180**: 2442–2449.
38) Wai, S.N., Mizunoe, Y., Takade, A., Kawabata, S.I., and Yoshida, S.I. 1998. *Vibrio cholerae* O1 strain TSI-4 produces the exopolysaccharide materials that determine

colony morphology, stress resistance, and biofilm formation. Appl. Environ. Microbiol. **64**: 3648–3655.
39) Wai, S.N., Mizunoe, Y., and Jass, J. 2003. Biofilm related infections on tissue surface, p. 97–117. *In* Jass, J., Walker, J.T., and Surman, S. (eds), Medical biofilms Vol. II: problems, detection and control, John Wiley & Sons, Ltd., London.
40) Watnick, P.I., and Kolter, R. 1999. Steps in the development of a *Vibrio cholerae* El Tor biofilm. Mol. Microbiol. **34**: 586–595.
41) Williams, V., and Fletcher, M. 1996. *Pseudomonas fluorescens* adhesion and transport through porous media are affected by lipopolysaccharide composition. Appl. Environ. Microbiol. **62**: 100–104.
42) Wimpenny, J. 2000. Structural determinants in biofilm formation, p. 35–49. *In* Evans, L.V. (ed), Biofilms: recent advances in their study and control, Harwood Academic Publishers, Amsterdam.
43) Yildiz, F.H., and Schoolnik, G.K. 1999. *Vibrio cholerae* O1 El Tor: identification of a gene cluster required for the rugose colony type, exopolysaccharide production, chlorine resistance, and biofilm formation. Proc. Natl. Acad. Sci. U.S.A. **96**: 4028–4033.

Available online at www.sciencedirect.com
SCIENCE DIRECT
Brain Research 1046 (2005) 24 – 31
BRAIN RESEARCH
www.elsevier.com/locate/brainres

Research report

Activation of presynaptic $GABA_A$ receptors increases spontaneous glutamate release onto noradrenergic neurons of the rat locus coeruleus

Hitoshi Koga[a], Hitoshi Ishibashi[a], Hideki Shimada[a], Il-Sung Jang[b], Tomoe Y. Nakamura[a], Junichi Nabekura[b,*]

[a]*Cellular and System Physiology, Graduate School of Medical Sciences, Kyushu University, Fukuoka 812-8582, Japan*
[b]*Department of Developmental Physiology, Division of Homeostatic Development, National Institute for Physiological Sciences, Okazaki 444-8585, Japan*

Accepted 15 March 2005
Available online 17 May 2005

Abstract

In order to further explore how GABA can modulate the excitability of noradrenergic neurons of the locus coeruleus (LC), we investigated the presence of $GABA_A$ receptors on glutamatergic nerve terminals and the functional consequences of their activation. We used mechanically dissociated immature rat LC neurons with adherent nerve terminals and patch-clamp recordings of spontaneous excitatory postsynaptic currents. Activation of presynaptic $GABA_A$ receptors by muscimol facilitated spontaneous glutamate release by activating tetrodotoxin-sensitive Na^+ channels and high-threshold Ca^{2+} channels. Bumetanide (10 μM), a potent blocker of Na^+–K^+–Cl^- cotransporter, diminished the muscimol-induced facilitatory action of glutamate release. Our results indicate that the Na^+–K^+–Cl^- cotransporter accumulates Cl^- inside the nerve terminals so that activation of presynaptic $GABA_A$ receptors causes depolarization. This $GABA_A$-receptor-mediated modulation of spontaneous glutamatergic transmission is another mechanism by which GABA and its analogues can regulate the excitability and activity of noradrenergic neurons in the LC.

Theme: Excitable membranes and synaptic transmission
Topic: Mechanisms of neurotransmitter release

Keywords: Spontaneous EPSC; NKCC; Muscimol; Presynaptic Ca^{2+} channels

1. Introduction

The locus coeruleus (LC) contains large clusters of noradrenaline-containing neurons (A6 cell group) which project widely throughout the central nervous system (CNS) [49]. The LC plays important roles in the control of cognitive and emotional processes, including attention and anxiety [7,13]. LC neurons typically spontaneously fire action potentials [3,50] and this firing rate is altered by a variety of sensory stimuli and is particularly modulated by the sleep–wake cycle [5,21]. LC neurons show their highest level of activity during active waking, decrease their firing frequency during slow wave sleep, and are almost silent during rapid eye movement sleep [4]. At a cellular level, the excitability of LC neurons is regulated by both excitatory and inhibitory synaptic inputs. For instance, the in vivo iontophoretic application of glutamate receptor agonists increases the firing frequency [8], whereas iontophoretic application of γ-aminobutyric acid (GABA) suppresses the activity of LC neurons [12]. However, the systemic or intracerebroventricular administration of GABA-mimetics has a facilitatory effect on central noradrenergic neurons [2,11] and enhances the catecholamine current measured by in vivo voltammetry [40].

GABA is the primary inhibitory neurotransmitter throughout the mammalian CNS. Activation of ionotropic $GABA_A$ receptors increases the Cl^- conductance of membrane. This results in postsynaptic hyperpolarization

* Corresponding author.
E-mail address: nabekura@nips.ac.jp (J. Nabekura).

0006-8993/$ - see front matter © 2005 Elsevier B.V. All rights reserved.
doi:10.1016/j.brainres.2005.03.026

in adult neurons, although in developing and injured neurons, Cl^- channel activation causes a depolarization because of the high intracellular Cl^- concentration [10,17,27,35]. These GABA-induced depolarizations can elevate the intracellular Ca^{2+} concentration via activation of voltage-dependent Ca^{2+} channels [29] and this is thought to contribute to synapse maturation. A $GABA_A$-receptor-mediated depolarization has also been observed in mature presynaptic nerve terminals [23,24,41,44]. In sensory afferent terminals, the activation of presynaptic $GABA_A$ receptors induces presynaptic inhibition of action-potential evoked transmitter release by inactivating Na^+ channels and/or shunting the presynaptic membrane potential [41,44]. In contrast, the presynaptic depolarization induced by $GABA_A$ receptor activation increases spontaneous transmitter release [23,24]. Such $GABA_A$-receptor-mediated presynaptic depolarization also results from a higher intraterminal Cl^- concentration, resulting from inwardly directed Cl^- transport mechanism such as the Na–K–Cl cotransporter (NKCC) [23,27,48].

Direct iontophoretic application of GABA to the LC in brain slices reduces the firing rate of rat LC neurons in a manner sensitive to the $GABA_A$ receptor blocker, bicuculline [45]. However, it is not clear whether this is mediated solely through postsynaptic $GABA_A$ receptors or whether presynaptic $GABA_A$ receptors also contribute. Capsaicin, for example, increases the activity of LC neurons by acting on presynaptic VR1 receptors to increase spontaneous glutamate release, without affecting either evoked release or without directly acting on LC neurons [31]. We therefore hypothesized that GABA might also affect LC noradrenergic neuron excitability by acting on glutamatergic presynaptic terminals. To test this, we studied the effects of the $GABA_A$ receptor agonist, muscimol, on spontaneous excitatory postsynaptic currents (sEPSCs) recorded in juvenile rat LC neurons which were mechanically isolated so as to retain adherent and functional presynaptic nerve terminals [1].

2. Experimental procedures

2.1. Preparation

Wistar rats (13–17 days old) were decapitated under pentobarbital sodium anesthesia (80 mg/kg, i.p.). The brain was quickly removed and sliced at a thickness of 380 μm using a microslicer (VT1000S; Leica, Nussloch, Germany). Slices were kept in the incubation medium (see below) saturated with 95% O_2 and 5% CO_2 at room temperature (21–24 °C) for at least 1 h before the mechanical dissociation. Slices were then transferred into a 35-mm culture dish (Primaria 3801; Becton Dickinson, Rutherford, NJ, USA), and the region of the LC was identified under a binocular microscope. Details of the mechanical dissociation have been recently reviewed [1].

All experiments were performed under guiding principles for care and use of animals approved by the Council to the Physiological Society of Japan.

2.2. Electrical measurements

The electrical measurements were performed using conventional whole-cell patch-clamp recordings at holding potentials of −60 to −65 mV. Membrane voltage was controlled, and currents recorded, with the use of a patch-clamp amplifier (EPC-7; List Medical, Darmstadt-Eberstadt, Germany). Patch pipettes were made from borosilicate capillary glass in two stages on a vertical pipette puller (PB-7, Narishige, Tokyo, Japan). The resistance between the recording pipettes filled with internal solution and the reference electrode was 4–6 MΩ. Neurons were visualized under phase contrast on an inverted microscope (Diaphot; Nikon, Tokyo, Japan). Current and voltage were continuously monitored on an oscilloscope and a pen recorder (WR3320, Graphtec, Tokyo, Japan). Membrane currents were filtered at 3 kHz (E-3201A; NF Electric Instruments, Tokyo, Japan), digitized at 6 kHz, and stored on a computer equipped with pCLAMP8.0 (Axon Instruments). All experiments were performed at room temperature (21–24 °C).

2.3. Immunostaining for tyrosine hydroxylase (TH) in dissociated LC neurons

We performed immunocytochemical experiments. Dissociated neurons were allowed to settle on to polyethlenimine (PEI)-coated, glass coverslips which were then transferred on to small strips of in a 35-mm culture dish. Coverslips were moved to parafilm sheet for immunocytochemistry. Neurons were fixed with 4% paraformaldehyde in phosphate-buffered saline (PBS) for 30 min at 4 °C, and were then washed with PBS. After treatment with 0.2% Triton X-100 for 5 min at room temperature, neurons were incubated with PBS containing 5% normal bovine serum for 30 min and then incubated with 1% normal bovine serum for 10 min. Neurons were subsequently incubated with PBS containing rabbit anti-tyrosine hydroxylase (TH) antibody (1:1000; Chemicon International) and 1% normal bovine serum for 1.5 h, and then with fluorescein isothiocyanate (FITC)-conjugated donkey anti-rabbit secondary antibody (1:150; Jackson ImmunoResearch Laboratories) for a further 1 h. Neurons were photographed through a microscope with a digital camera (Carl Zeiss, Germany).

2.4. Data analysis

Spontaneous EPSCs were detected and analyzed using the MiniAnalysis program (Synaptosoft, Decatur, GA). Spontaneous events were initially detected automatically, using an amplitude threshold of 3 pA, and then visually

accepted or rejected on the basis of the rise and decay times. Events with brief rise times (0.5–1.5 ms), and with decay times that were well fitted by a single-exponential function were selected for further analysis. The amplitude and interevent intervals of large numbers of sEPSCs obtained from a single neuron were examined by constructing all-point cumulative probability distributions and compared using the Kolmogorov–Smirnov test. Values of $P < 0.05$ were considered significant. Differences in mean sEPSC amplitude and frequency under different conditions were tested with Student's paired two-tailed t test using their absolute values. Values of $P < 0.05$ were considered significant.

2.5. Solutions

The composition of incubation solutions was (in mM): 124 NaCl, 2.5 KCl, 1.2 KH_2PO_4, 24 $NaHCO_3$, 2 $CaCl_2$, 1 $MgCl_2$, and 10 glucose saturated with 95% O_2 and 5% CO_2. The standard external solution consisted of (in mM) 150 NaCl, 2.5 KCl, 2 $CaCl_2$, 1 $MgCl_2$, 10 HEPES, and 10 glucose. This standard external solution was adjusted to pH 7.4 with tris(hydroxymethyl)aminomethane (Tris-base). The ionic composition of the internal (patch pipette) solution was (in mM) 145 Cs-methanesulfonate, 5 tetraethylammonium-Cl, 5 CsCl, 2 EGTA, and 10 HEPES. The pH was adjusted to 7.2 with Tris-base.

2.6. Drugs

Drugs used in the present study were bicuculline (Tocris Cookson, Avonmouth, UK), diazepam (Wako, Tokyo, Japan), muscimol, tetrodotoxin, bumetanide (Sigma, St Louis, MO, USA), ω-conotoxin-MVIIC, and nilvadipine (Peptide Institute, Osaka, Japan). Drugs were applied using 'Y-tube system', which enables rapid solution exchange.

3. Results

3.1. Spontaneous EPSCs in noradrenergic neurons

In order to firstly identify the noradrenergic neurons amongst the acutely dissociated LC neurons, we imaged TH-immunoreactivity. As shown in Fig. 1A, TH-positive neurons had a relatively large soma (≧40 μm) and multiple dendritic processes, while TH-negative neurons were smaller in size (≦20 μm) and often with bipolar dendrites (Fig. 1A). Current deflections representing spontaneous action potentials were typically seen at a frequency of 1.5–5 Hz in cell-attached recordings from these large neurons (Fig. 1B). This observation is consistent with previous reports that LC noradrenergic neurons discharge spontaneous action potentials at 1–4 Hz [3,13]. Thus, the following electrophysiological experiments were only performed on LC neurons with large somas and multiple dendrites.

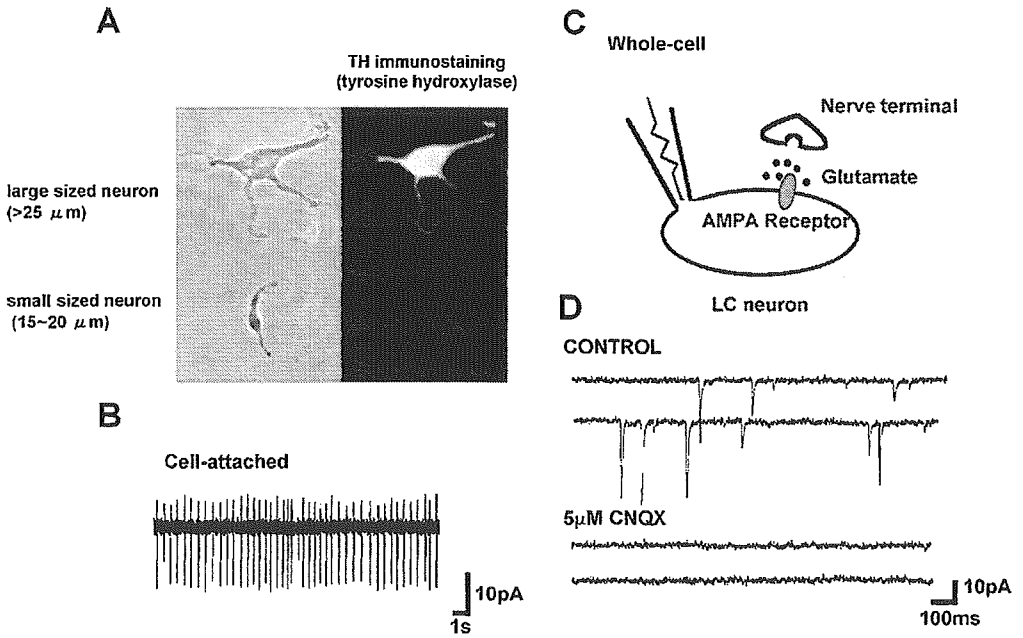

Fig. 1. Spontaneous EPSCs in noradrenergic neurons. (A) TH immunostaining of acutely dissociated LC neurons. Phase contrast (left) and TH immunostainings (right) of the dissociated LC neurons. The TH-positive neurons had a relatively large soma and were multipolar in shape, whereas the TH-negative neuron had a small soma and were often bipolar. (B) Current deflections representing spontaneous firing of action potentials in a large LC neuron recorded in the cell-attached patch-clamp recording mode. (C) Schematic representation of synaptic current recording from the dissociated neuron with adherent nerve terminals. (D) Effect of CNQX on spontaneous postsynaptic currents. Recordings were performed at a holding potential (V_H) of −61 mV using the conventional whole-cell patch recording configuration. The traces were representative of 5 neurons.

The noradrenergic neurons of the LC receive not only glutamatergic inputs, but also GABAergic inputs [43]. To distinguish between $GABA_A$ receptors on the glutamatergic presynaptic terminals synapsing onto the isolated LC neurons from $GABA_A$ receptors on the postsynaptic membrane, we dialyzed the cells with an ATP-free pipette solution for at least 30 min before applying muscimol. This causes a rapid rundown of postsynaptic $GABA_A$ receptor responses [23,42] and allows us to selectively investigate the effects of presynaptic $GABA_A$ receptor activation. In addition, the V_H of the LC neurons was adjusted to about −60 mV which was close to the reversal potential of the muscimol-induced postsynaptic currents in our experimental conditions ($[Cl^-]_i$; 10 mM, $[Cl^-]_o$; 161 mM). Under these conditions, all the spontaneous postsynaptic currents were reversibly inhibited by 5 μM CNQX (Fig. 1D), indicating that they were sEPSCs mediated by non-NMDA type glutamate receptors.

3.2. $GABA_A$-receptor-mediated modulation of spontaneous EPSCs

As shown in Fig. 2, the application of muscimol (1 μM) increased the frequency of sEPSCs from 1.63 ± 0.18 to 3.37 ± 0.36 Hz ($P < 0.001$, $n = 22$). The cumulative distribution of sEPSC interevent intervals was shifted to the left by muscimol, whereas the cumulative distribution of sEPSC amplitude was not affected. (Fig. 2B). These results indicate that muscimol acts presynaptically to facilitate spontaneous glutamate release at these synapses.

To confirm that muscimol facilitates sEPSC frequency via $GABA_A$ receptors, we investigated the effect of bicuculline, a $GABA_A$ receptor antagonist, on this response. The facilitation of sEPSC frequency elicited by 1 μM muscimol was completely blocked in the presence of 5 μM bicuculline (Fig. 3). We also examined the effect of diazepam, a $GABA_A$ receptor allosteric potentiator on the muscimol response (Fig. 4). In 5 neurons tested, a subthreshold dose of muscimol (0.5 μM) had no significant affect on sEPSC frequency. The sEPSC frequency in the absence and presence of 0.5 μM muscimol was 1.47 ± 0.18 and 2.09 ± 0.46 Hz ($n = 5$, $P = 0.112$), respectively. Although diazepam (1 μM) itself did not affect the sEPSC frequency, the co-application of both 0.5 μM muscimol and 1 μM diazepam increased sEPSC frequency from 1.15 ± 0.36 to 3.11 ± 0.60 Hz ($P < 0.01$, $n = 5$).

3.3. Involvement of voltage-dependent Na^+ and Ca^{2+} channels in muscimol-induced facilitation of release

We next examined the possible mechanisms underlying the $GABA_A$-receptor-mediated facilitation of sEPSC frequency. First, we investigated the effect of tetrodotoxin (TTX), a voltage-dependent Na^+ channel blocker. As shown in Fig. 5, application of TTX reduced the basal sEPSC frequency from 1.38 ± 0.26 to 0.64 ± 0.196 Hz. In the presence of TTX, the facilitation of sEPSC frequency by muscimol (1 μM) was completely abolished, indicating a critical contribution of tetrodotoxin-sensitive Na^+ channels to the muscimol response.

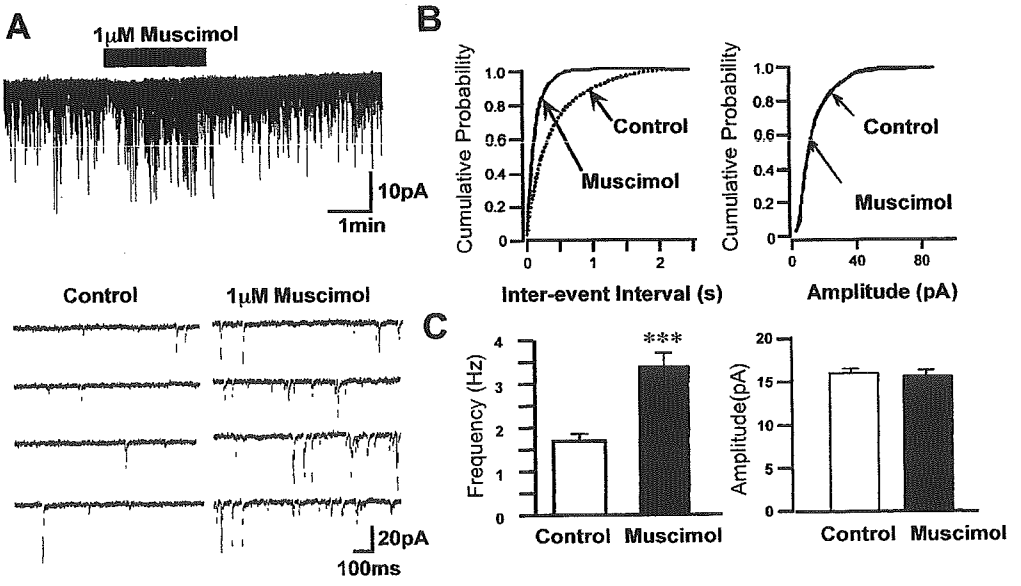

Fig. 2. The effect of muscimol on spontaneous EPSCs. (A) A typical recording of spontaneous EPSCs before, during, and after application of 1 μM muscimol. A portion of currents during control recordings and in the presence of muscimol are shown at greater resolution in the lower panel. (B) Cumulative distributions of interevent intervals (left) and spontaneous EPSC amplitudes (right) in control conditions and in the presence of 1 μM muscimol. All data come from the same neuron as shown in panel A. (C) The mean frequency and amplitude of spontaneous EPSCs recorded under control conditions and in the presence of muscimol (1 μM). The mean data come from 22 neurons. ***$P < 0.001$.

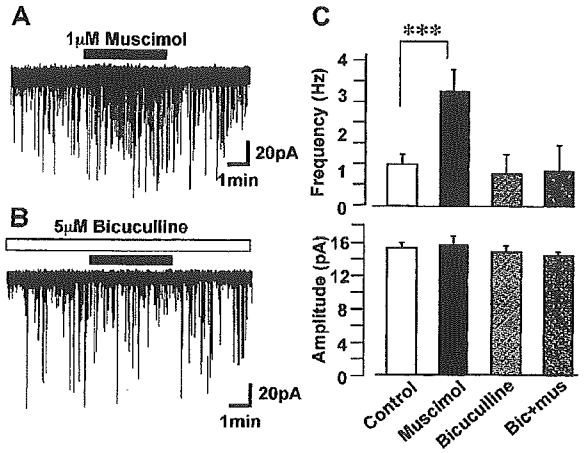

Fig. 3. Inhibition by bicuculline of the muscimol-induced increase in spontaneous EPSC frequency. (A and B) Typical current traces of spontaneous EPSCs observed before, during, and after application of 1 μM muscimol in the absence (A) or continued presence (B) of 5 μM bicuculline. (C) Histograms showing the mean affects of bicuculline on the muscimol response. Data have been averaged from 3 neurons. Bic: bicuculline; Mus: muscimol; ***$P < 0.01$.

We next examined the effect of Cd^{2+}, a general blocker of voltage-dependent Ca^{2+} channels, on the muscimol response. Application of Cd^{2+} (100 μM), by itself, reduced basal sEPSC frequency to 36.2 ± 12.8% (n = 3) of the control rate ($P < 0.01$). In the presence of Cd^{2+}, the muscimol-induced facilitation was completely abolished (Fig. 6). However, because Cd^{2+} itself may directly block $GABA_A$ receptors [28], we also tested the effects of nilvadipine, an L-type Ca^{2+} channel antagonist [22], and ω-conotoxin-MVIIC, a blocker of N- and P/Q-type Ca^{2+} channels [20]. Both nilvadipine (0.3 μM) and ω-conotoxin-MVIIC (3 μM) reduced the basal sEPSC frequency, to 56.3 ± 6.9 (n = 5) and 44.7 ± 5.8% (n = 4) of control, respectively. In the presence of 0.3 μM nilvadipine, however, muscimol (1 μM) still increased sEPSC frequency, to 197.2 ± 27.2% (n = 7; Fig. 6). This is comparable to the extent of facilitation seen in the absence of nilvadipine. In contrast, 3 μM ω-conotoxin-MVIIC completely abolished the muscimol action (Fig. 6). These results suggest the contribution of N- and/or P/Q-type high-voltage-activated Ca^{2+} channels to the muscimol-induced facilitation of glutamate release.

3.4. Contribution of the Na–K–Cl cotransporter to the muscimol response

Since the muscimol-induced facilitation of sEPSC frequency depended critically on the activation of voltage-dependent Na^+ and Ca^{2+} channels, it is reasonable to conclude that the activation of presynaptic $GABA_A$ receptors depolarizes the glutamatergic nerve terminals. This may result from Cl^- efflux, which implies that the intraterminal Cl^- concentration is maintained higher than that predicted for a passive distribution. If this is indeed the case, a higher intraterminal Cl^- concentration might be established by some inwardly directed Cl^- transport systems, such as

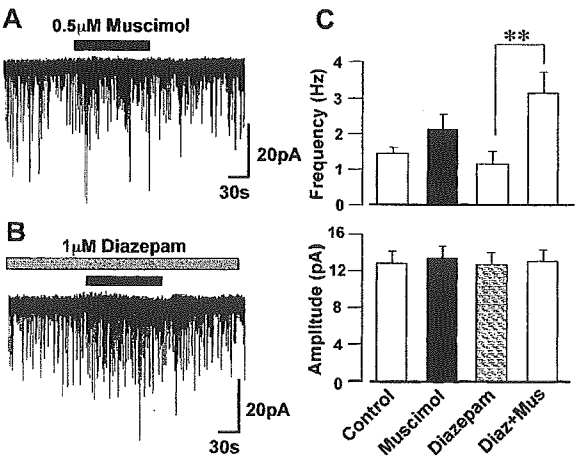

Fig. 4. Effect of diazepam on the muscimol-induced increase in spontaneous EPSC frequency. (A and B) Typical current traces of spontaneous EPSCs observed before, during, and after application of 0.5 μM muscimol in the absence (A) or continued presence (B) of 1 μM diazepam. (C) Histograms showing the mean affects of diazepam on the muscimol response. Data have been averaged from 5 neurons. Diaz: diazepam; Mus: muscimol; **$P < 0.01$.